A Compact 2-D FDFD Method for Modeling Microstrip Structures With Nonuniform Grids and Perfectly Matched Layer

Jiunn-Nan Hwang

Abstract—**Full-wave analysis of the microstrip structures is performed by using the compact two-dimensional (2-D) finite-difference frequency-domain (FDFD) method with nonuniform grids and perfectly matched layer (PML). The use of nonuniform grids can significantly reduce the computational matrix size. Less memory and CPU time are required as comparing with the original compact 2-D FDFD method. For the analysis of the microstrip structures with an absorbing boundary condition, the compact 2-D FDFD method with PML is presented. The performances of different PML thickness are studied. Numerical examples are presented to demonstrate the accuracy and efficiency of this method.**

Index Terms—**Compact two-dimensional (2-D) finite difference frequency domain (FDFD), nonuniform grids, perfectly matched layer (PML).**

I. Introduction

Accurately modeling the dispersion characteristics of a microstrip is important at the design stage. This procedure can be fulfilled by full-wave modeling approach. Among the available full-wave techniques, the finite-difference time-domain (FDTD) method has been widely used as an accurate way to predict the electromagnetic behavior of many guided-wave structures. To solve propagation problems, some research has introduced the dispersive boundary condition or high order boundary condition [1]–[3]. In these approaches, the phase of electric-field components at different locations are compared and the propagation constant can be extracted with knowledge of wave propagation between these locations. Another study [4] was performed by extracting equivalent-circuit components of a microstrip to determine the propagation constant and characteristic impedance. However, these approaches are limited to extract single-mode parameters due to the Fourier transform limit. The studies described in [5], [6] employed new methods with high-resolution signal-processing techniques and have the advantage of extracting multimode parameters. Unfortunately, when the dispersion parameters are very close to each other or extracting data at very low frequency, this method requires long simulation time.

The finite-difference frequency-domain (FDFD) method can also be used to calculate the dispersion parameters [7], [8]. In the existing FDFD method, the eigenfrequency can be extracted with a given propagation constant. Recently, a new compact two-dimensional (2-D) FDFD method [9], [10] was introduced to determine the propagation constant of guided-wave structures. Unlike the existing FDFD methods, the propagation constant can be extracted with a given frequency. This method can be used to accurately extract propagation constants of dominant and higher order modes. However, when studying guided-wave structures with fine geometry features, the computational matrix will be increased if uniform grids are used. Another problem is the boundary condition in [9] is a perfect electric conductor (PEC). The compact 2-D FDFD method with an absorbing boundary condition has not yet been proposed.

In this paper, we propose a novel compact 2-D FDFD method with nonuniform grids and a perfectly matched layer to determine the propagation constant. In this approach, the simulation domain can be reduced significantly with nonuniform grids [11], [12]. We will demonstrate the advantage of this method by computing the dispersion characteristics of electrically large microstrip structures. The propagation problem in open space can be solved by introducing the perfectly matched layer (PML) concept [13], [14]. The PML equation for the compact 2-D FDFD method, which yields an eigenequation, is presented. We will compare the absorbing efficiency and computer burden of different PML thicknesses. The performances of the simulation results are evaluated.

II. Compact 2-D FDFD Method

The compact 2-D FDFD method can find the propagation constant β with a given frequency k_0. In this method, only four transverse fields are involved in the final equation. The compact 2-D FDFD equations are given by [9]

$$\begin{aligned}\frac{\beta}{k_0}E_x(i,j) = &-\frac{1}{k_0^2\varepsilon_r\Delta x\Delta y}\\ &\times\Big[H_x(i,j-1)-H_x(i+1,j-1)-H_x(i,j)\\ &+H_x(i+1,j)\Big]+\frac{1}{k_0^2\varepsilon_r\Delta x^2}H_y(i-1,j)\\ &+\left(1-\frac{2}{k_0^2\varepsilon_r\Delta x^2}\right)H_y(i,j)\\ &+\frac{1}{k_0^2\varepsilon_r\Delta x^2}H_y(i+1,j) \qquad (1)\end{aligned}$$

Manuscript received February 3, 2004; revised May 6, 2004 and June 29, 2004.

The author is with the Department of Communication Engineering, National Chiao Tung University, Hsinchu 300, Taiwan, R.O.C. (e-mail: emigma.cm91g@nctu.edu.tw).

Digital Object Identifier 10.1109/TMTT.2004.840569

$$\begin{aligned}\frac{\beta}{k_0}E_y(i,j) = &-\frac{1}{k_0^2\varepsilon_r\Delta y^2}H_x(i,j-1)\\ &-\left(1-\frac{2}{k_0^2\varepsilon_r\Delta y^2}\right)H_x(i,j)\\ &-\frac{1}{k_0^2\varepsilon_r\Delta y^2}H_x(i,j+1)+\frac{1}{k_0^2\varepsilon_r\Delta x\Delta y}\\ &\times\Big[H_y(i-1,j)-H_y(i,j)-H_y(i-1,j+1)\\ &\quad+H_y(i,j+1)\Big]\end{aligned} \tag{2}$$

$$\begin{aligned}\frac{\beta}{k_0}H_x(i,j) = &\frac{1}{k_0^2\Delta x\Delta y}\Big[E_x(i-1,j)-E_x(i,j)\\ &\qquad -E_x(i-1,j+1)+E_x(i,j+1)\Big]\\ &-\frac{1}{k_0^2\Delta x^2}E_y(i-1,j)\\ &-\left(\varepsilon_r-\frac{2}{k_0^2\Delta x^2}\right)E_y(i,j)\\ &-\frac{1}{k_0^2\Delta x^2}E_y(i+1,j)\end{aligned} \tag{3}$$

$$\begin{aligned}\frac{\beta}{k_0}H_y(i,j) = &\frac{1}{k_0^2\Delta y^2}E_x(i,j-1)+\left(\varepsilon_r-\frac{2}{k_0^2\Delta y^2}\right)E_x(i,j)\\ &+\frac{1}{k_0^2\Delta y^2}E_x(i,j+1)-\frac{1}{k_0^2\Delta x\Delta y}\\ &\times\Big[E_y(i,j-1)-E_y(i+1,j-1)-E_y(i,j)\\ &\quad+E_y(i+1,j)\Big]\end{aligned} \tag{4}$$

where Δx and Δy are the grid space in the x- and y- directions.

Equation (1)–(4) can be concluded as an eigenproblem as

$$[A]\cdot\{x\} = \lambda\{x\} \tag{5}$$

where $\lambda = \beta/k_0$, $\{x\} = \{E_x, E_y, H_x, H_y\}^T$, and $[A]$ is a sparse matrix and its matrix coefficients are listed in (1)–(4).

To save the memory resource, the computational matrix can be decreased by using coarse grids in simulation. However, the grid size will influence the accuracy of numerical results. In the FDTD method [15], the grid size should be smaller than $\lambda_u/10$ in the material medium, where λ_u is the wavelength of the highest frequency in the simulated frequency spectrum. In Section II, we will propose a new scheme to reduce the computational matrix while the numerical accuracy can still be maintained.

III. Compact 2-D FDFD With Nonuniform Grids

In the compact 2-D FDFD method, the computational domain depends on the size of the modeled structure. To simulate guided-wave structures with fine geometry features, fine grids are often used to accurately model the local field phenomena. This results in global refinement of the mesh density if uniform grids are used. Such a high level of refinement will increase the computational matrix size. To reduce the computational matrix size, the compact 2-D FDFD method with nonuniform grids is presented.

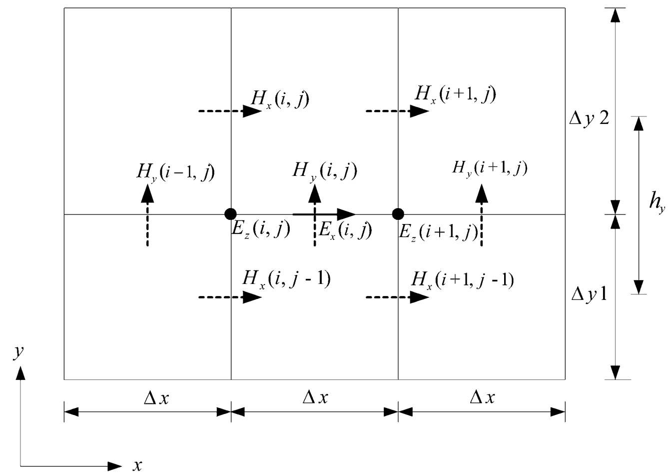

Fig. 1. Spatial arrangement of the field components with 2-D nonuniform grids.

Fig. 1 shows the spatial layout of the field components with 2-D nonuniform grids. When Yee's grid is reduced to a compact 2-D grid, we can obtain

$$H_y(i,j) = \frac{\beta}{k_0}E_x(i,j) - j\frac{1}{k_0\Delta x}\Big[E_z(i+1,j)-E_z(i,j)\Big] \tag{6}$$

$$\begin{aligned}\varepsilon_r E_z(i,j) = &-j\frac{1}{k_0\Delta x}\Big[H_y(i,j)-H_y(i-1,j)\Big]\\ &+j\frac{1}{k_0 h_y}\Big[H_x(i,j)-H_x(i,j-1)\Big]\end{aligned} \tag{7}$$

where h_y is set as the average of the grid size in the two regions, i.e., $h_y = (\Delta y1 + \Delta y2)/2$.

After substituting E_z into (6), we can obtain

$$\begin{aligned}\frac{\beta}{k_0}E_x(i,j) = &-\frac{1}{k_0^2\varepsilon_r\Delta x h_y}\\ &\times\Big[H_x(i,j-1)-H_x(i+1,j-1)-H_x(i,j)\\ &\quad+H_x(i+1,j)\Big]+\frac{1}{k_0^2\varepsilon_r\Delta x^2}H_y(i-1,j)\\ &+\left(1-\frac{2}{k_0^2\varepsilon_r\Delta x^2}\right)H_y(i,j)\\ &+\frac{1}{k_0^2\varepsilon_r\Delta x^2}H_y(i+1,j).\end{aligned} \tag{8}$$

Other field components can also be derived with similar procedures. When using the nonuniform grids, the grid space Δx and Δy in (1)–(4) are replaced by fine or coarse grid space depending on the electromagnetic fields' positions.

IV. Compact 2-D FDFD Method With PML Implementation

The PML equations for the compact 2-D FDFD method are presented here. The original unsplit form of the PML equations in the frequency domain are given by [14]

$$\begin{aligned}&(jwu_0+\sigma_y^*)H_x(i,j)\\ &\quad = -j\beta E_y(i,j) - \frac{\partial}{\partial y}E_z(i,j) + \frac{\sigma_z^*-\sigma_y^*}{jwu_0+\sigma_z^*}j\beta E_y(i,j)\end{aligned} \tag{9}$$

$$(jwu_0+\sigma_z^*)H_y(i,j) = +j\beta E_x(i,j)+\frac{\partial}{\partial x}E_z(i,j)-\frac{\sigma_x^*-\sigma_z^*}{jwu_0+\sigma_x^*}\frac{\partial}{\partial x}E_z(i,j) \tag{10}$$

$$(jwu_0+\sigma_x^*)H_z(i,j) = \frac{\partial}{\partial y}E_x(i,j)-\frac{\partial}{\partial x}E_y(i,j)-\frac{\sigma_y^*-\sigma_x^*}{jwu_0+\sigma_y^*}\frac{\partial}{\partial y}E_x(i,j) \tag{11}$$

$$(jw\varepsilon_0\varepsilon_r+\sigma_y)E_x(i,j) = +j\beta H_y(i,j)+\frac{\partial}{\partial y}H_z(i,j)-\frac{\sigma_z-\sigma_y}{jw\varepsilon_0\varepsilon_r+\sigma_z}j\beta H_y(i,j) \tag{12}$$

$$(jw\varepsilon_0\varepsilon_r+\sigma_z)E_y(i,j) = -j\beta H_x(i,j)-\frac{\partial}{\partial x}H_z(i,j)+\frac{\sigma_x-\sigma_z}{jw\varepsilon_0\varepsilon_r+\sigma_x}\frac{\partial}{\partial x}H_z(i,j) \tag{13}$$

$$(jw\varepsilon_0\varepsilon_r+\sigma_x)E_z(i,j) = -\frac{\partial}{\partial y}H_x(i,j)+\frac{\partial}{\partial x}H_y(i,j)+\frac{\sigma_y-\sigma_x}{jw\varepsilon_0\varepsilon_r+\sigma_y}\frac{\partial}{\partial y}H_x(i,j) \tag{14}$$

where σ and σ^* denote electric and magnetic conductivity, respectively.

The waves in the z- direction do not need to be absorbed, i.e., $\sigma_z = \sigma_z^* = 0$. After some algebraic manipulations, (9)–(14) become the following forms:

$$jwu_0H_x(i,j) = -j\beta E_y(i,j)-\frac{\partial}{\partial y}E_z(i,j)\frac{1}{\left(1-j\frac{\sigma_y^*}{wu_0}\right)} \tag{15}$$

$$jwu_0H_y(i,j) = +j\beta E_x(i,j)+\frac{\partial}{\partial x}E_z(i,j)\frac{1}{\left(1-j\frac{\sigma_x^*}{wu_0}\right)} \tag{16}$$

$$jwu_0H_z(i,j) = \frac{\partial}{\partial y}E_x(i,j)\frac{1}{\left(1-j\frac{\sigma_y^*}{wu_0}\right)} - \frac{\partial}{\partial x}E_y(i,j)\frac{1}{\left(1-j\frac{\sigma_x^*}{wu_0}\right)} \tag{17}$$

$$jw\varepsilon_0\varepsilon_rE_x(i,j) = +j\beta H_y(i,j)+\frac{\partial}{\partial y}H_z(i,j)\frac{1}{\left(1-j\frac{\sigma_y}{w\varepsilon_0\varepsilon_r}\right)} \tag{18}$$

$$jw\varepsilon_0\varepsilon_rE_y(i,j) = -j\beta H_x(i,j)-\frac{\partial}{\partial x}H_z(i,j)\frac{1}{\left(1-j\frac{\sigma_x}{w\varepsilon_0\varepsilon_r}\right)} \tag{19}$$

$$jw\varepsilon_0\varepsilon_rE_z(i,j) = -\frac{\partial}{\partial y}H_x(i,j)\frac{1}{\left(1-j\frac{\sigma_y}{w\varepsilon_0\varepsilon_r}\right)} + \frac{\partial}{\partial x}H_y(i,j)\frac{1}{\left(1-j\frac{\sigma_x}{w\varepsilon_0\varepsilon_r}\right)}. \tag{20}$$

By normalizing the field components with a square root of the free-space wave impedance such that $H' = H\cdot\sqrt{\eta_0}$ and $E' = E/\sqrt{\eta_0}$, we can obtain

$$H_x(i,j) = -\frac{\beta}{k_0}E_y(i,j)+j\frac{1}{k_0\Delta y}\Big[E_z(i,j+1)-E_z(i,j)\Big] \times\frac{1}{\left(1-j\frac{\sigma_y^*}{wu_0}\right)} \tag{21}$$

$$H_y(i,j) = +\frac{\beta}{k_0}E_x(i,j)-j\frac{1}{k_0\Delta x}\Big[E_z(i+1,j)-E_z(i,j)\Big] \times\frac{1}{\left(1-j\frac{\sigma_x^*}{wu_0}\right)} \tag{22}$$

$$H_z(i,j) = -j\frac{1}{k_0\Delta y}\Big[E_x(i,j+1)-E_x(i,j)\Big]\frac{1}{\left(1-j\frac{\sigma_y^*}{wu_0}\right)} + j\frac{1}{k_0\Delta x}\Big[E_y(i+1,j)-E_y(i,j)\Big] \times\frac{1}{\left(1-j\frac{\sigma_x^*}{wu_0}\right)} \tag{23}$$

$$\varepsilon_rE_x(i,j) = +\frac{\beta}{k_0}H_y(i,j)-j\frac{1}{k_0\Delta y}\Big[H_z(i,j)-H_z(i,j-1)\Big] \times\frac{1}{\left(1-j\frac{\sigma_y}{w\varepsilon_0\varepsilon_r}\right)} \tag{24}$$

$$\varepsilon_rE_y(i,j) = -\frac{\beta}{k_0}H_x(i,j)+j\frac{1}{k_0\Delta x}\Big[H_z(i,j)-H_z(i-1,j)\Big] \times\frac{1}{\left(1-j\frac{\sigma_x}{w\varepsilon_0\varepsilon_r}\right)} \tag{25}$$

$$\varepsilon_rE_z(i,j) = +j\frac{1}{k_0\Delta y}\Big[H_x(i,j)-H_x(i,j-1)\Big] \times\frac{1}{\left(1-j\frac{\sigma_y}{w\varepsilon_0\varepsilon_r}\right)}-j\frac{1}{k_0\Delta x} \times\Big[H_y(i,j)-H_y(i-1,j)\Big]\frac{1}{\left(1-j\frac{\sigma_x}{w\varepsilon_0\varepsilon_r}\right)}. \tag{26}$$

E_z and H_z are substituted into (21) and (22) and (24) and (25), respectively, the PML equations for the compact 2-D FDFD method can be obtained as (27)–(30) as follows:

$$\frac{\beta}{k_0}E_x(i,j) = -\frac{1}{\left(1-j\frac{\sigma_x^*}{wu_0}\right)\left(1-j\frac{\sigma_y}{w\varepsilon_0\varepsilon_r}\right)k_0^2\varepsilon_r\Delta x\Delta y} \times\Big[H_x(i,j-1)-H_x(i+1,j-1)-H_x(i,j) + H_x(i+1,j)\Big] + \frac{1}{\left(1-j\frac{\sigma_x^*}{wu_0}\right)\left(1-j\frac{\sigma_x}{w\varepsilon_0\varepsilon_r}\right)k_0^2\varepsilon_r\Delta x^2}H_y(i-1,j)$$

$$+\left(1-\frac{2}{\left(1-j\frac{\sigma_x^*}{wu_0}\right)\left(1-j\frac{\sigma_x}{w\varepsilon_0\varepsilon_r}\right)k_0^2\varepsilon_r\Delta x^2}\right)H_y(i,j)+\frac{1}{\left(1-j\frac{\sigma_x^*}{wu_0}\right)\left(1-j\frac{\sigma_x}{w\varepsilon_0\varepsilon_r}\right)k_0^2\varepsilon_r\Delta x^2}H_y(i+1,j) \tag{27}$$

$$\begin{aligned}\frac{\beta}{k_0}E_y(i,j) &= -\frac{1}{\left(1-j\frac{\sigma_y^*}{wu_0}\right)\left(1-j\frac{\sigma_y}{w\varepsilon_0\varepsilon_r}\right)k_0^2\varepsilon_r\Delta y^2}H_x(i,j-1)\\ &\quad-\left(1-\frac{2}{\left(1-j\frac{\sigma_y^*}{wu_0}\right)\left(1-j\frac{\sigma_y}{w\varepsilon_0\varepsilon_r}\right)k_0^2\varepsilon_r\Delta y^2}\right)\\ &\quad\times H_x(i,j)-\frac{1}{\left(1-j\frac{\sigma_y^*}{wu_0}\right)\left(1-j\frac{\sigma_y}{w\varepsilon_0\varepsilon_r}\right)k_0^2\varepsilon_r\Delta y^2}\\ &\quad\times H_x(i,j+1)\\ &\quad+\frac{1}{\left(1-j\frac{\sigma_y^*}{wu_0}\right)\left(1-j\frac{\sigma_x}{w\varepsilon_0\varepsilon_r}\right)k_0^2\varepsilon_r\Delta x\Delta y}\\ &\quad\times\Big[H_y(i-1,j)-H_y(i,j)-H_y(i-1,j+1)\\ &\qquad+H_y(i,j+1)\Big]\end{aligned} \tag{28}$$

$$\begin{aligned}\frac{\beta}{k_0}H_x(i,j) &= \frac{1}{\left(1-j\frac{\sigma_x}{w\varepsilon_0\varepsilon_r}\right)\left(1-j\frac{\sigma_y^*}{wu_0}\right)k_0^2\Delta x\Delta y}\\ &\quad\times\Big[E_x(i-1,j)-E_x(i,j)-E_x(i-1,j+1)\\ &\qquad+E_x(i,j+1)\Big]\\ &\quad-\frac{1}{\left(1-j\frac{\sigma_x}{w\varepsilon_0\varepsilon_r}\right)\left(1-j\frac{\sigma_x^*}{wu_0}\right)k_0^2\Delta x^2}E_y(i-1,j)\\ &\quad-\left(\varepsilon_r-\frac{2}{\left(1-j\frac{\sigma_x}{w\varepsilon_0\varepsilon_r}\right)\left(1-j\frac{\sigma_x^*}{wu_0}\right)k_0^2\Delta x^2}\right)\\ &\quad\times E_y(i,j)\\ &\quad-\frac{1}{\left(1-j\frac{\sigma_x}{w\varepsilon_0\varepsilon_r}\right)\left(1-j\frac{\sigma_x^*}{wu_0}\right)k_0^2\Delta x^2}E_y(i+1,j)\end{aligned} \tag{29}$$

$$\begin{aligned}\frac{\beta}{k_0}H_y(i,j) &= \frac{1}{\left(1-j\frac{\sigma_y}{w\varepsilon_0\varepsilon_r}\right)\left(1-j\frac{\sigma_y^*}{wu_0}\right)k_0^2\Delta y^2}E_x(i,j-1)\\ &\quad+\left(\varepsilon_r-\frac{2}{\left(1-j\frac{\sigma_y}{w\varepsilon_0\varepsilon_r}\right)\left(1-j\frac{\sigma_y^*}{wu_0}\right)k_0^2\Delta y^2}\right)\\ &\quad\times E_x(i,j)\\ &\quad+\frac{1}{\left(1-j\frac{\sigma_y}{w\varepsilon_0\varepsilon_r}\right)\left(1-j\frac{\sigma_y^*}{wu_0}\right)k_0^2\Delta y^2}E_x(i,j+1)\\ &\quad-\frac{1}{\left(1-j\frac{\sigma_y}{w\varepsilon_0\varepsilon_r}\right)\left(1-j\frac{\sigma_x^*}{wu_0}\right)k_0^2\Delta x\Delta y}\\ &\quad\times\Big[E_y(i,j-1)-E_y(i+1,j-1)-E_y(i,j)\\ &\qquad+E_y(i+1,j)\Big].\end{aligned} \tag{30}$$

The directional electric conductivity in the PML is defined as

$$\sigma_u=\sigma_m\left(\frac{u}{\delta}\right)^n \tag{31}$$

$$\sigma_m=-\frac{(n+1)\varepsilon_0 c}{2\delta}\ln R_{\mathrm{th}} \tag{32}$$

where u is either x or y, δ is the thickness of the PML, and σ_m is the maximum electric conductivity at the outer side of the PML.

When studying the surface of conductors, it can be done by inserting the boundary condition $E_z = 0$ into (21)–(26) and systematically modifying (27)–(30) accordingly. For example, $E_z(i+1,j)=0$ in (22) and (27) will become

$$\begin{aligned}\frac{\beta}{k_0}E_x(i,j) &= -\frac{1}{\left(1-j\frac{\sigma_x^*}{wu_0}\right)\left(1-j\frac{\sigma_y}{w\varepsilon_0\varepsilon_r}\right)k_0^2\varepsilon_r\Delta x\Delta y}\\ &\quad\times\Big[H_x(i,j-1)-H_x(i,j)\Big]\\ &\quad+\frac{1}{\left(1-j\frac{\sigma_x^*}{wu_0}\right)\left(1-j\frac{\sigma_x}{w\varepsilon_0\varepsilon_r}\right)k_0^2\varepsilon_r\Delta x^2}H_y(i-1,j)\\ &\quad+\left(1-\frac{1}{\left(1-j\frac{\sigma_x^*}{wu_0}\right)\left(1-j\frac{\sigma_x}{w\varepsilon_0\varepsilon_r}\right)k_0^2\varepsilon_r\Delta x^2}\right)\\ &\quad\times H_y(i,j).\end{aligned} \tag{33}$$

V. Numerical Experiments

Numerical examples are used to verify the proposed method. In the first example, a dual-plane triple microstrip line on an anisotropic substrate, shown in Fig. 2, is studied. The modeled structure reported in [6] consists of 40×24 uniform grids, and the corresponding sparse matrix size $[A]$ is $\{3968\times 3968\}$. The computational domain can be reduced with nonuniform grids. The configuration of the modeled structure with nonuniform grids is shown in Fig. 3. The fine grid Δ is chosen as 0.25 mm and the coarse grids $\Delta x1$, $\Delta x2$, $\Delta y1$, and $\Delta y2$ are chosen as 0.4, 0.46, 0.4, and 0.48 mm, respectively. As shown in Fig. 4, the simulation results of the normalized effective dielectric constant are compared with those in [16]. Good agreement can be

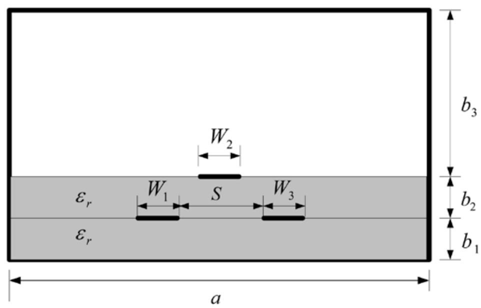

Fig. 2. Cross section of dual-plane triple microstrip lines. $a = 10.0$ mm, $b_1 = b_2 = 1.0$ mm, $b_3 = 4.0$ mm, $\varepsilon_{rx} = 9.4$, $\varepsilon_{ry} = 11.6$, $\varepsilon_{rz} = 9.4$, $W_1 = W_2 = W_3 = 1.0$ mm, and $S = 2.0$ mm.

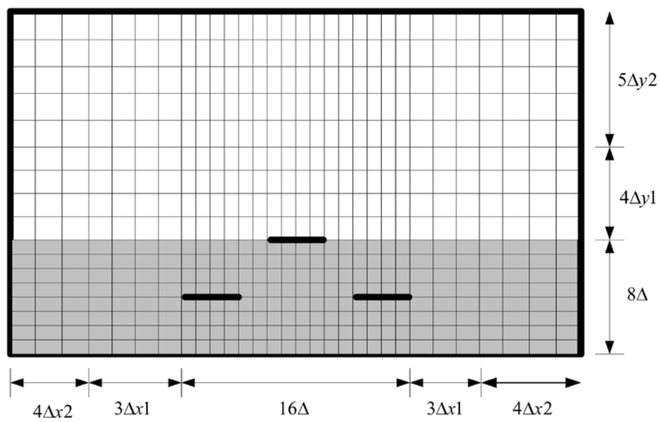

Fig. 3. Cross section of dual-plane triple microstrip lines with nonuniform grids.

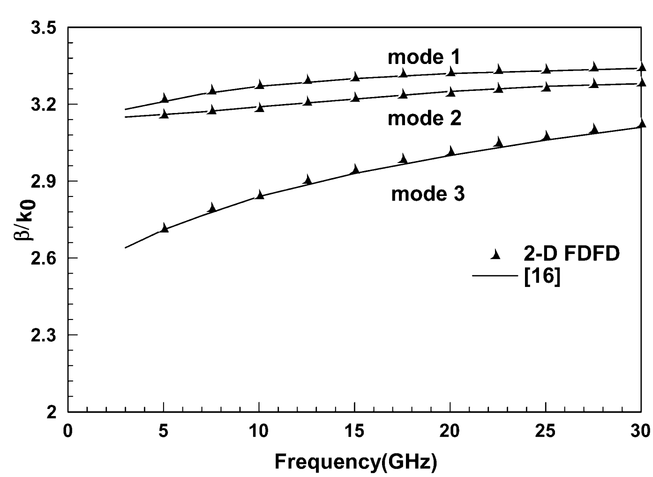

Fig. 4. Simulation results of the normalized propagation constants for dual-plane triple microstrip lines.

observed. The computational matrix size has been reduced to be $\{2134 \times 2134\}$ with nonuniform grids.

The second analyzed structure is a coupled microstrip lines with finite strip thickness t, as shown in Fig. 5. We use fine grids to model the strip thickness and coarse grids in other regions. The simulation results are shown in Fig. 6 and are compared with those in [17]. Good agreement is also reached.

To verify the proposed PML equations for the compact 2-D FDFD method, a microstrip line with an absorbing boundary condition is studied. As shown in Fig. 7, the PML is implemented on the sidewalls of the microstrip structure.

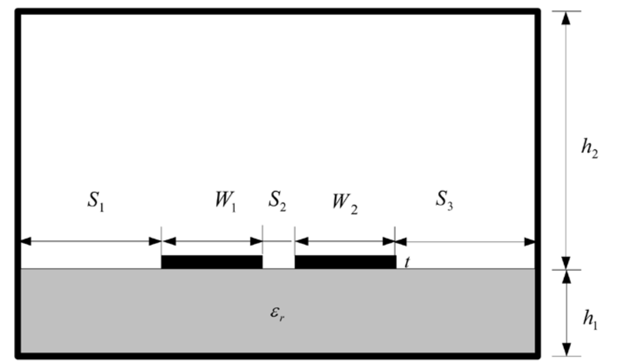

Fig. 5. Cross section of parallel coupled microstrip lines with finite strip thickness. $\varepsilon_r = 12.5$. $W_1 = W_2 = S_2 = h_1 = 0.6$ mm, $h_2 = 10$ mm, and $S_1 = S_3 = 6$ mm.

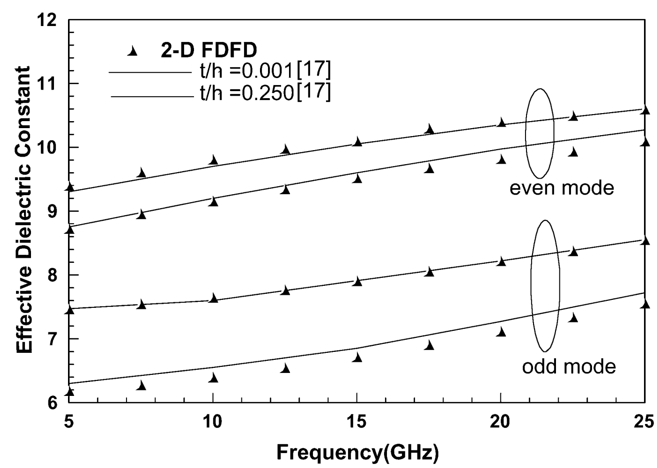

Fig. 6. Modeled effective dielectric constant for a coupled microstrip lines.

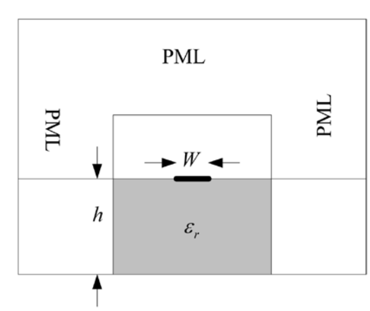

Fig. 7. Cross section of the computation domain for a microstrip line. $W = 0.5$ mm, $h = 1.5$ mm, and $\varepsilon_r = 9.4$.

To reduce the computational matrix, the thinner PML can be used and the absorbing efficiency must still be maintained. It has been found in [18] that the theoretical reflection coefficient $R_{\rm th}$ and power n need to be properly chosen to achieve small reflection. The thicker the PML, the smaller the chosen $R_{\rm th}$ should be. After deciding upon the value of $R_{\rm th}$, the optimum range of n can be predicted. In this study, the PML thickness of five, six, eight, and ten cells are studied. The $R_{\rm th}$ are chosen to be 10^{-5}, 10^{-6}, 10^{-7}, and 10^{-9}, respectively. The n of the five-cell-thick PML is chosen to be 2.0. When the PML thickness is larger than six cells, n is chosen between 2.5–2.7. We increase the distance

TABLE I
MODELED RESULTS WITH DIFFERENT PML THICKNESS AND ITS CORRESPONDING MATRIX SIZE

	REFERENCE DATA	5PML	6PML	8PML	10PML
10G	2.616	2.6116-i0.1578	2.6134-i0.0641	2.6173-i0.0203	2.6157-i0.008
20G	2.7635	2.7371+i0.0262	2.7612-i0.0148	2.7635+i0.0043	2.7649-i0.0001
30G	2.8624	2.8686-i0.0045	2.8639-i0.0031	2.8620+i0.0004	2.8626-i0.00006
SPARSE MATRIX SIZE	1814×1814	650×650	804×804	1160×1160	1580×1580

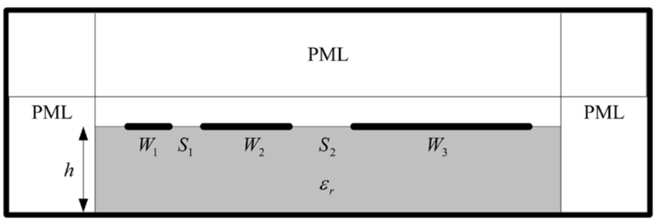

Fig. 8. Cross section of an asymmetric three-line microstrip lines with PML implementation. $h = 0.635$ mm, $W_1 = 0.3$ mm, $S_1 = 0.2$ mm, $W_2 = 0.6$ mm, $S_2 = 0.4$ mm, $W_3 = 1.2$ mm, and $\varepsilon_r = 9.8$.

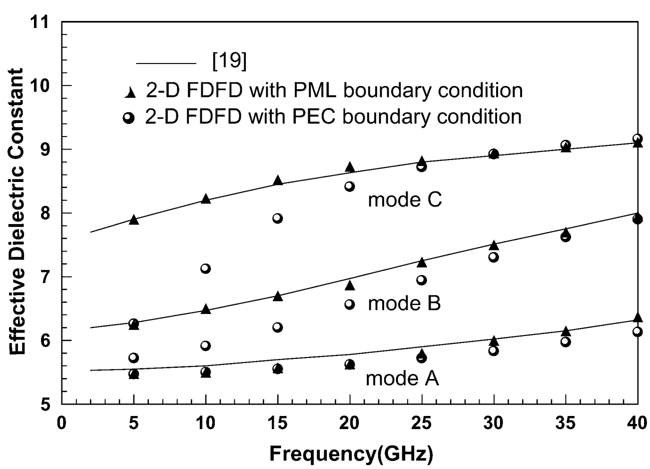

Fig. 9. Modeled effective dielectric constant for an asymmetric microstrip line.

between the microstrip line and PEC boundary as reference data to verify the PML absorbing efficiency. The distance is ten times the width of the microstrip line. The sparse matrix size of reference data is $\{1814 \times 1814\}$. The simulated normalized propagation constant β/k_0 is shown in Table I. Since the PML equations for the compact 2-D FDFD method are complex, the simulation results are also complex. The real part is the normalized propagation constant and the imaginary part is the loss due to the PML. The imaginary part will be decreased with an increase in the PML thickness. Comparing the simulation results of different PML thickness with the reference data, it is found that the performance of the six-cell PML can already achieve accurate results and sparse matrix size can also be significantly reduced.

The second analyzed structure is an asymmetric three-line coupled microstrip lines, as shown in Fig. 8. The modeled structure with the PML boundary condition and PEC boundary condition are both studied. The thickness of the PML is six cells. Both the computational matrix size are $\{2754 \times 2754\}$. Fig. 9 shows the simulated effective dielectric constant. From the simulation results, it can be found that the dispersion parameters of the PEC boundary condition are smaller than those in [19]. Accurate results can be obtained by implementing a PML boundary condition.

VI. CONCLUSION

In this paper, the compact 2-D FDFD method with nonuniform grids and a PML have been presented. When studying electrically large transmission-line systems, the use of nonuniform grids can significantly reduce the computational domain. The eigenform PML equations for the compact 2-D FDFD method are proposed to study the microstrip structure in open space. From simulation results, it is found that the performance of the six-cell PML can achieve accurate results with properly choosing PML reflection parameters. Numerical examples have been presented to demonstrate the efficiency and accuracy of this method.

REFERENCES

[1] X. Zhang and K. K. Mei, "Time-domain finite difference approach to the calculation of the frequency-dependent characteristics of microstrip discontinuities," *IEEE Trans. Microw. Theory Tech.*, vol. 36, no. 12, pp. 1775–1787, Dec. 1988.
[2] X. Zhang, J. Fang, K. K. Mei, and Y. Liu, "Calculation of the dispersive characteristics of microstrips by the time-domain finite difference method," *IEEE Trans. Microw. Theory Tech.*, vol. 36, no. 4, pp. 263–267, Apr. 1988.
[3] Z. Bi, K. Wu, C. Wu, and J. Litva, "A dispersive boundary condition for microstrip component analysis using FD-TD method," *IEEE Trans. Microw. Theory Tech.*, vol. 40, no. 4, pp. 774–777, Apr. 1992.
[4] L. L. Liu, M. Mah, and J. Cook, "An equivalent circuit approach for microstrip component analysis using the FDTD method," *IEEE Microw. Guided Wave Lett.*, vol. 8, no. 10, pp. 330–332, Oct. 1998.
[5] Y. X. Wang and H. Ling, "Multimode parameter extraction for multiconductor transmission lines via single-pass FDTD and signal-processing," *IEEE Trans. Microw. Theory Tech.*, vol. 46, no. 1, pp. 89–96, Jan. 1998.
[6] F. Liu, J. Schutt-Aine, and J. Chen, "Full-wave analysis and modeling of multiconductor transmission lines via 2-D FDTD and signal-processing techniques," *IEEE Trans. Microw. Theory Tech.*, vol. 50, no. 2, pp. 570–577, Feb. 2002.
[7] H. Y. D. Yang, "Finite difference analysis of 2-D photonic crystals," *IEEE Trans. Microw. Theory Tech.*, vol. 44, no. 12, pp. 2688–2695, Dec. 1996.
[8] C. L. D. S. S. Sobrinho and A. J. Giarola, "Analysis of an infinite array of rectangular anisotropic dielectric waveguides using finite-difference method," *IEEE Trans. Microw. Theory Tech.*, vol. 40, no. 5, pp. 1021–1025, May 1992.
[9] Y.-J. Zhao, K.-L. Wu, and K. M. Cheng, "A compact 2-D full-wave finite-difference frequency-domain method for general guided wave structures," *IEEE Trans. Microw. Theory Tech.*, vol. 50, no. 7, pp. 1844–1848, July 2002.

[10] M.-L. Liu and Z. Chen, "A direct computation of propagation constant using compact 2-D full-wave eigen based finite-difference frequency-domain technique," in *Proc. Int. Computational Electromagnetics Applications Conf.*, Beijing, China, Nov. 1999, pp. 78–81.
[11] P. Monk and E. Suli, "A convergence analysis of Yee's scheme on nonuniform grids," *SIAM J. Numer. Anal.*, vol. 31, pp. 393–412, 1994.
[12] P. Monk, "Error estimates for Yee's method on nonuniform grids," *IEEE Trans. Magn.*, vol. 30, no. 9, pp. 3200–3203, Sep. 1994.
[13] J. P. Berenger, "A perfectly matched layer for the absorbing of electromagnetic waves," *J. Comput. Phys.*, vol. 114, pp. 185–200, Oct. 1994.
[14] R. Mittra and U. Peekl, "A new look at the perfectly matched layer (PML) concept for reflectionless absorbing of electromagnetic waves," *IEEE Microw. Guided Wave Lett.*, vol. 1. 5, no. 5, pp. 330–332, Mar. 1995.
[15] A. Talflove, *Computational Electrodynamics: The Finite-Difference Time-Domain Method*. Norwood, MA: Artech House, 1995.
[16] M. S. Alam, M. Koshiba, K. Hirayama, and Y. Hayashi, "Hybrid-mode analysis of multilayered and multiconductor transmission lines," *IEEE Trans. Microw. Theory Tech.*, vol. 45, no. 2, pp. 205–211, Feb. 1997.
[17] J.-T. Kuo and T. Itoh, "Hybrid-mode computation of propagation and attenuation characteristics of parallel coupled microstrips with finite metallization thickness," *IEEE Trans. Microw. Theory Tech.*, vol. 45, no. 2, pp. 274–280, Feb. 1997.
[18] Z. Wu and J. Fang, "Numerical implementation and performance of perfectly matched layer boundary condition for waveguide structures," *IEEE Trans. Microw. Theory Tech.*, vol. 43, no. 12, pp. 2676–2683, Dec. 1995.
[19] V. K. Tripathi and H. Lee, "Spectral domain computation of the apparent characteristic impedances and multiport parameters of multiple coupled microstrip lines," *IEEE Trans. Microw. Theory Tech.*, vol. 37, no. 1, pp. 215–221, Jan. 1989.

Jiunn-Nan Hwang was born on June 23, 1978, in MiaoLi, Taiwan, R.O.C. He received the B.S.E.E. and M.S.E.E. degrees from the National Sun Yat-Sen University, Kaohsiung, Taiwan, R.O.C., in 2000 and 2002, respectively, and is currently working toward the Ph.D. degree in communication engineering at the National Chiao Tung University, Hsinchu, R.O.C.

His research interests include the electromagnetic modeling for electromagnetic compatibility (EMC)/electromagnetic interference (EMI) problem and applications for metamaterials.